JOURNAL OF CHEMICAL & ENGINEERING DATA

Article

pubs.acs.org/jced

Kinetic, Isotherm, and Thermodynamic Studies of the Adsorption of Methyl Orange from Aqueous Solution by Chitosan/Alumina Composite

Jixiang Zhang,*[,†] Qiuxiang Zhou,[†] and Lailiang Ou[‡]

[†]Department of Chemistry, Langfang Teachers' College, Hebei 065000, China

[‡]Key Laboratory of Bioactive Materials of Ministry of Education, Institute of Molecular Biology, Nankai University, Tianjin 300071, China

ABSTRACT: Alumina, a support material, was loaded with chitosan to form a chitosan/alumina composite (CA) and was utilized for removing sulfonated azo-dye methyl orange (MO) from aqueous media in this study. The adsorbents were characterized by Fourier transform infrared (FTIR) spectra to confirm that chitosan was successfully immobilized on alumina, and some functional groups were successfully introduced into the surface of alumina after modification. The effects of pH, the amount of adsorbent, initial concentration, time, and temperature were studied in batch experiments. The experimental data were analyzed by Langmuir and Freundlich adsorption isotherms. Thermodynamic parameters such as ΔG^{o}, ΔH^{o}, and ΔS^{o} have also been evaluated, and it has been found that the sorption process was spontaneous and exothermic in nature. Pseudofirst-order and pseudosecond-order kinetic models were used to fit the experimental data. Kinetic parameters, rate constants, equilibrium adsorption capacities, and related correlation coefficients for each kinetic model were calculated and discussed. It revealed that the adsorption of MO could be described by the pseudosecond-order equation, suggesting that the adsorption process is presumably chemisorption.

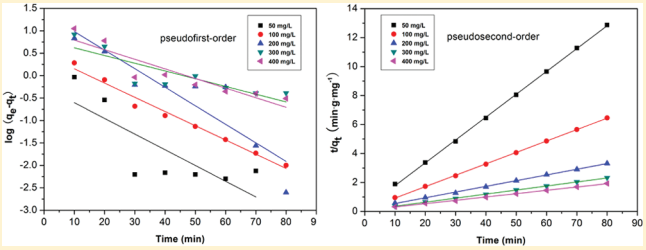

1. INTRODUCTION

Different synthetic dyes used in various industries such as textile, leather, paint, and so forth produce the highly visible wastewater effluents.[1,2] Some of these dyes are toxic and arouse a serious threat to environment. The discharge of dyes into water resources even in a small amount can affect aquatic life and the food web. Azo dyes are most widely used for natural and synthetic fiber dyeing and printing and also in paints, plastics, rubber, and so on. Under special conditions, they can decompose to produce about 20 kinds of carcinogenic aromatic amines and change human DNA structure to result in induced lesions and cancer.[3] Wastewaters with azo dyes are extensively discharged, and azo dyes are usually present in high concentration and varied compositions. Some recent research takes sulfonated azo-dye methyl orange (MO) as a model dye,[4−7] which is the most commonly used substance as an acid−base indicator. The investigation of the removal of MO from aqueous solution may be useful for further research and practical applications in azo-dye wastewater treatment.

In recent years, several wastewater treatment methods including chemical oxidation,[8−10] filtration,[11−13] coagulation and flocculation,[14−16] and adsorption with active carbon[17−19] have been developed for treating wastewater containing dye. Each of these methods has their own advantages and disadvantages. Among the mentioned methods, the adsorption technique is quite popular due to its simplicity and high efficiency. However, active carbon is high-cost, and disposal of the used carbon is difficult. Therefore, it is attractive to find other absorbents with high efficiency, low-cost, availability, and easy design. A number of nonconventional, low-cost adsorbents have been used for the removal of dyes in the past years,[20−29] which usually are natural inorganic minerals or industrial and agricultural waste materials. In addition, natural polymeric materials have drawn considerable attention because they are biodegradable, nontoxic, and friendly to environment.

Chitosan (CS) is the *N*-deacetylated derivative of chitin and the second most plentiful natural biopolymer. CS contains reactive hydroxyl (−OH) groups and amino ($-NH_2$) groups that have the potential to bind with heavy metal ions and dye materials. However, pure chitosan tends to agglomerate and form a gel in aqueous media, causing most of the hydroxyl and amino groups' loss of ability to react with metals and dyes. Physically and chemically modified CS can be used as adsorbent for treatment of industry effluents containing dyes as well as for metal ion extraction from wastewater.[30−37] In the present study, chitosan/alumina composite, coating chitosan as a thin layer onto an alumina support, increases the accessibility of its binding sites and improves the mechanical stability. The objective of the present work is to introduce a new adsorbent CA to examine its effectiveness in removing azo-dye MO from

Received: September 15, 2011
Accepted: December 14, 2011
Published: December 23, 2011

aqueous solution. The effect of pH, the amount of dried adsorbent, initial concentration, time, and temperature were studied in batch experiments. The adsorption kinetics, isotherms, and thermodynamics of interactions for MO dye onto the composite were also discussed.

2. EXPERIMENTAL SECTION

2.1. Materials. Chitosan (CS, degree of deacetylation: 90.0 %, average molecular weight is $8{\cdot}10^5$, L.N.: 110215) was supplied by Shanghai Lanji Biotechnology Development Co., Ltd., China. Alumina (for chromatographic use, 100 to 200 mesh size, L.N.: 070703) was obtained from the Shanghai Wusi Chemical Reagent Co., Ltd., China. Glacial acetic acid and sodium hydroxide was purchased from Tianjin Chemical Reagent Co., Ltd., China. The molecular formula of MO (Beijing Chemical Works, China, L.N.: 020613) is $C_{14}H_{14}N_3NaO_3S$, and the molecular structure is shown in Figure 1. Agents used were all of analytical grade, and all solutions were prepared with deionized water.

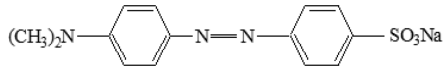

Figure 1. Chemical structure of MO.

2.2. Preparation and Characterization of Adsorbents. CA composite was manufactured according to a previous report with slight modifications.[38] An aqueous solution of CS was prepared by dissolving 2.00 g of CS in 250 mL of deionized water containing 2.50 mL of glacial acetic acid and stirred with a electric stirrer until the chitosan was completely dissolved. Then, alumina (7.00 g) was added to the CS solution, and the mixture was stirred at 1200 rpm for 4 h. The upper clear liquid was decanted, and the product CS-Al_2O_3 (CA) composite was washed with deionized water three times to remove the unreacted CS. Finally, the product was dried in a vacuum drying oven for 6 h at 70 °C to get the CA absorbent. Raw CS, CA adsorbents, and MO loaded on CA were analyzed using a Fourier transform infrared spectrometer (Shimadzu, IRPrestige-21 spectrophotometer, Japan) under ambient conditions. The spectra were recorded from 4000 to 400 cm^{-1} using KBr discs. These three samples were analyzed by using a scanning electron microscope (KYKY Technology Development Ltd., KYKY-2800B SEM, China) to study the morphologies. The surface area analysis was implemented by surface area analyzer (Micromeritics Instrument Corporation, ASAP 2010-M, USA) based on the Brunauer–Emmett–Teller (BET) equation.

2.3. Preparation and Analysis of Dye Solutions. A stock solution of MO dye was prepared (1 $g{\cdot}L^{-1}$) by dissolving a required amount of dye powder in deionized water. The stock solution was diluted with deionized water to obtain the desired concentration ranging from (50 to 400) $mg{\cdot}L^{-1}$. The concentration of MO in the experimental solution was determined from the calibration curve prepared by measuring absorbance of different determined concentrations of MO solutions at a wavelength of 464 nm (MO has a maximum absorbency at a wavelength of 464 nm) using a UV–vis spectrophotometer (UV-2550, Shimadzu, Japan). The pH of solution was measured with a Rex pH meter using a combined glass electrode (model E-201-C, China).

2.4. Adsorption Experiments. Adsorption experiments were conducted by varying pH, initial MO concentration, CA dose, contact time, and temperature under the aspects of thermodynamic study, adsorption isotherms, and adsorption kinetics. All batch experiments were carried out in 250 mL Erlenmeyer flasks and performed on a thermostatted shaker (THZ-82A, Ronghua, China) with a shaking of 120 rpm, and the temperature was controlled during each experiment to be within 0.1 °C. The pH of MO solution was adjusted at a desired value by adding 0.1 $mol{\cdot}L^{-1}$ NaOH or HCl. For kinetic studies, 50 mL of MO solutions of different concentrations, that is, from (50 to 400) $mg{\cdot}L^{-1}$ with 8 $g{\cdot}L^{-1}$ adsorbent was agitated in the water bath shaker. The mixture was agitated at 120 rpm at 25 °C, and the contact time was varied from (0 to 100) min. At predetermined times, the samples were withdrawn from the shaker, and the dye solution was separated from the adsorbent by centrifuging at 4000 rpm for 10 min. The absorbances of the supernatants were measured at the wavelength 464 nm. Dye concentration was calculated from the calibration curve. The thermodynamic study were performed by varying temperature from (25 to 55) °C using 8 $g{\cdot}L^{-1}$ CA added to 50 mL of MO solution in 250 mL flasks. The flasks were shaken at 120 rpm for 90 min. All of the experiments were performed in duplicate. The amount of dye adsorbed onto CA, q_e ($mg{\cdot}g^{-1}$), was calculated by the following mass balance relationship:

$$q_e = \frac{(C_i - C_e)V}{W} \quad (1)$$

where C_i and C_e are the initial and equilibrium concentrations ($mg{\cdot}L^{-1}$) of MO dye solution, respectively; V is the volume (L); and W is the mass (g) of the adsorbent.

2.5. Desorption Experiments. To investigate the desorption ability of adsorbed MO from the adsorbent CA, desorption experiments were carried out as follows: After adsorption with the 200 $mg{\cdot}L^{-1}$ MO solution, the MO loaded adsorbents were separated from the unadsorbed MO solution. Then the effects of time and temperature on desorption were studied. The sample was stirred with 50 mL of deionized water, and the concentrations of MO were analyzed as before. The desorption ratio of MO was then calculated as the ratio of the amount of MO to the amount of initially adsorbed MO.

2.6. Experimental Uncertainties. The uncertainty of the analytical balance used for weighing the amounts of materials was less than 0.1 %. The volume of the solution was measured with an uncertainty of less than 0.1 % in all of the cases. Therefore, the uncertainty in the determination of the initial solution concentration was less than 0.14 %. The uncertainty of spectrophotometric analysis was less than 0.25 %, and the dilution of the high concentration solution to the concentration in the range of standard curve has an uncertainty of less than 0.22 %. Thus, the precision of calculated values of MO solution concentration was estimated to be within 0.33 %.

3. RESULTS AND DISCUSSION

3.1. Characterization of CA. Pure chitosan tends to agglomerate and form a gel in aqueous media, causing most of the amino groups' loss of ability to react with dyes. The adsorption capacity of CA depends upon the surface area as well as the number of active groups on the surface. The free amino groups on the surface of CA could combine with the sulfonic group of MO to form a salt bond, thus leading to molecular adsorption. Information on functional groups would give insight to the adsorption capability of the CA. The FT-IR spectra of the CS, CA, and MO loaded on CA is shown in

dx.doi.org/10.1021/je2009945 | J. Chem. Eng.Data 2012, 57, 412–419

Figure 2. OH and NH stretching is between (3100 and 3500) cm^{-1}. The peak at 2927 cm^{-1} is due to the C−H stretching of

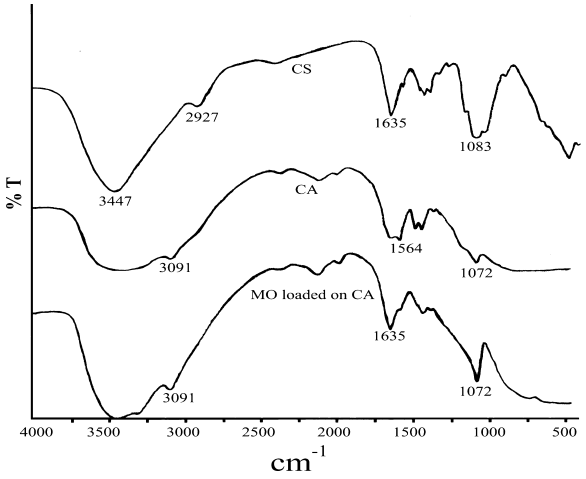

Figure 2. FT-IR spectrum of CS, CA, and MO loaded on CA.

CH_2 groups for CS. For CA and MO loaded on CA, the C−H stretching peak appears to be a obvious shift to the higher wavenumber, which is due to the combination of CS with alumina. The broad bands near 3447 cm^{-1} indicates the presence of hydroxyl groups and amino groups. However, the broad bands near 3447 cm^{-1} present different shapes. Among the three bands, the band of CS is sharp, CA is broad, and MO load on CA is in between. The result showed that the free amino groups of CS are less than those of CA. However, the 3447 cm^{-1} broad peak after adsorption turns to sharp compared to CA, which exhibit some amino groups reacting with the sulfonic groups of MO. In addition, the peak at 1564 cm^{-1} is the N−H deformation vibration of amino groups. The peak is obvious for CA, and it almost disappears when MO is loaded on CA. The result also indicates that the amino groups react with sulfonic groups to form salt bonds:

$$MO - SO_3^- + CA - NH_3^+ \rightarrow MO - SO_3^- \cdots NH_3^+ - CA$$

The analysis of microstructures of the materials is shown in Figure 3a−c, which presents scanning electron micrographs. The obtained micrographs detail the morphology of each material. It is noticed that the porous or crevice structure is obvious for alumina for chromatographic use (Figure 3a). The micromorphology of the chitosan powder is shown in Figure 3b. The structure characteristics of amorphous polymers can be seen evidently. Chitosan can dissolve in the dilute solution of acetic acid and has good film-forming properties. CA composite is prepared after the mixture of CS solution and alumina is stirred for a long enough time. Chitosan can form a layer of film on the surface of the alumina carrier, and those microporous and crevices of alumina are covered with the film (Figure 3c). The chitosan film on the surface of CA composite is rather thin compared with the pure chitosan powder. The forming-film chitosan no longer tends to agglomerate, and the number of free amino groups increases in CA compared to CS. The amino groups on the surface of the chitosan film can react more effectively with sulfonic groups. The effective use of free amino groups is enhanced greatly.

The values of specific surface area for alumina and CA with BET surface area analysis are 143.071 $m^2 \cdot g^{-1}$ and 141.884 $m^2 \cdot g^{-1}$, respectively. By contrast, the specific surface area of CA composite is slightly smaller than that of alumina. The reason causing this result can be interpreted that the chitosan film covers most of the porous and crevices.

3.2. Effect of pH. The solution pH has an important influence on the dye adsorption due to its influence on the surface properties of the CA and ionization of the MO molecule. The effect of pH on removal of MO dye from aqueous solution at various solution pH is shown in Figure 4. From the figure, it can be seen that the maximum removal of dye is observed at pH 6. A low pH leads to an increase in H^+ ion concentration in the system, and the ionization of SO_3^- ions decreases with increased H^+. Moreover, the color range of MO is pH 3.1 to 4.4, and the accuracy is affected by the change of maximum adsorption wavelength of MO when pH is less than 5. As the CA surface is positively charged at low pH, a significantly strong electrostatic attraction appears between the positively charged CA surface and anionic dye molecule leading to maximum adsorption of the dye. As the pH of the system increases, decreased NH_3^+ leads to lower adsorption. Furthermore, the surface site on the CA does not favor the adsorption of anionic dye molecules due to the electrostatic repulsion.

3.3. Effect of Adsorbent Dose. The study of the effect of adsorbent dose is necessary to observe the maximum adsorption with the minimum possible amount of adsorbent. The plot between the % MO removal against adsorbent dose is shown in Figure 4. It can be seen that the % MO removal increases with increased adsorbent dose. The % MO removal increases from 92.84 to 99.23 % for an increase in adsorbent dose from (1 to 12) $g \cdot L^{-1}$. At higher CA to MO concentration ratios, there is a higher % MO removal. This is because a fixed dose of CA can only adsorb a certain amount of dye. Therefore, the higher the adsorbent dosage, the larger the volume of effluent can be purified with a fixed dosage of CA. Initially, a rapid increase of adsorption with the increasing adsorbent

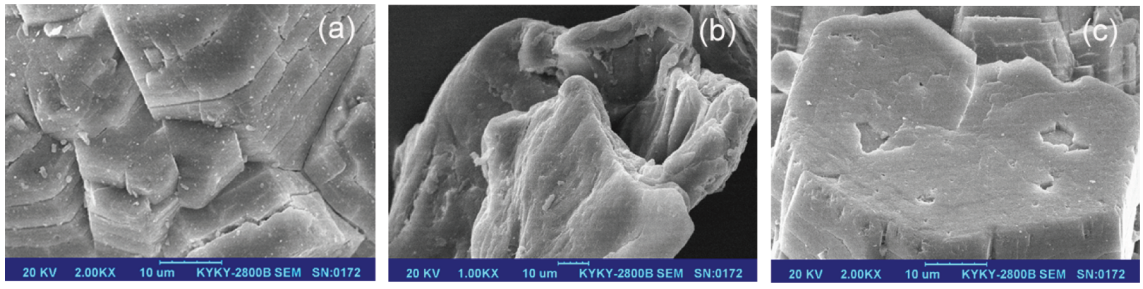

Figure 3. Scanning electron micrographs: (a) Alumina, (b) CS, and (c) CA.

dx.doi.org/10.1021/je2009945 | J. Chem. Eng.Data 2012, 57, 412−419

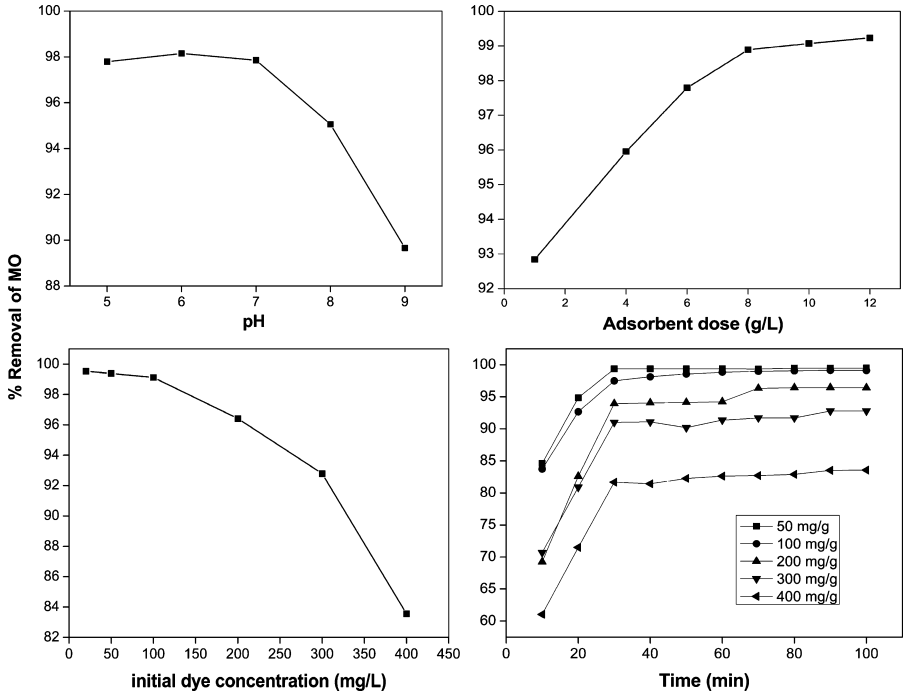

Figure 4. Effect of pH, adsorbent dose, initial dye concentration, and contact time on the MO removal.

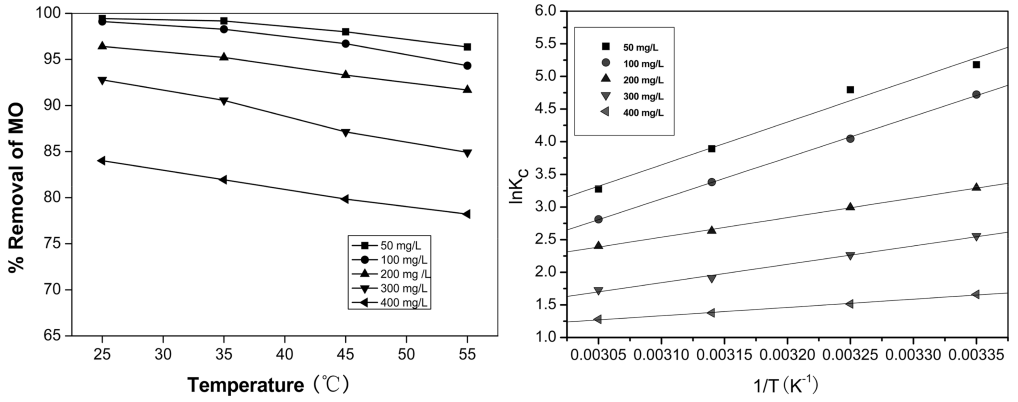

Figure 5. Effect of temperature on the MO removal and thermodynamic study.

dosage is attributed to the availability of more adsorption sites. After the critical dose (about 8 g·L^{-1}), the rate of dye removal increases much more slowly (only from 98.89 % to 99.23 %). This can be attributed to the splitting effect of flux (concentration gradient) between adsorbent and adsorbate.

3.4. Effect of Initial Dye Concentration. The initial dye concentration plays an important role in the adsorption capacity. The effect of initial dye concentration in the range of (20 to 400) mg·L^{-1} on MO removal using CA was carried out, and the results are shown in Figure 4. The initial dye concentration provides the necessary driving force to overcome the resistance of mass transfer from the aqueous phase to the solid phase. The higher the initial concentration is, the greater the driving force becomes. The increase in initial dye concentration also enhances the interaction between MO and CA. Therefore, an increase in initial concentration of MO enhances the adsorption capability of CA for MO. While the % MO removal was found to be 99.53 % for a 20 mg·L^{-1} initial concentration, it was 83.55 % for 400 mg·L^{-1}.

3.5. Effect of Contact Time. The contact time for the removal of MO by the CA at concentrations in the range of (50 to 400) mg·L^{-1} for the adsorbent dose of 8 g·L^{-1} showed rapid adsorption of dye in the first 30 min. Thereafter, the adsorption rate decreased, and the adsorption reached equilibrium in about 90 min as shown in Figure 4. It can be explained that the chitosan surface was progressively blocked by the dyes reaching pseudoequilibrium in about 90 min. Generally, the adsorption capacity increases with time and reaches a constant value where no more dye is removed from the solution at some point in time. At this point, the dye amount being adsorbed onto the material is in a state of dynamic equilibrium with the dye amount desorbed from the adsorbent. The differences in the adsorption values after 90 min were very small, so further experiments were conducted for a 90 min contact time only.

3.6. Effect of Temperature. The removal of MO using CA was investigated as a function of temperature, and the result was given in Figure 5. The experiments were performed at different temperatures of (25, 35, 45, and 55) °C for the initial MO concentrations of (50 to 400) mg·L^{-1} at a constant

dx.doi.org/10.1021/je2009945 | J. Chem. Eng.Data 2012, 57, 412−419

Table 1. Thermodynamic Parameters for the Adsorption of MO onto CA

initial MO concn.	ΔH^o	ΔS^o	ΔG^o/kJ·mol^{-1}			
mg·L^{-1}	kJ·mol^{-1}	J·mol^{-1}·K^{-1}	25 °C	35 °C	45 °C	55 °C
50	−54.528	−138.729	−13.166	−11.779	−10.392	−9.004
100	−52.675	−137.329	−11.730	−10.356	−8.983	−7.610
200	−25.013	−56.450	−8.182	−7.617	−7.053	−6.488
300	−23.370	−57.143	−6.333	−5.762	−5.190	−4.619
400	−10.540	−21.587	−4.148	−3.933	−3.719	−3.504

Table 2. Parameters of Langmuir's and Freundlich's Equations

	Langmuir			Freundlich		
	parameters			parameters		
temperature	K_L	q_m		K_F		
°C	L·mg^{-1}	mg·g^{-1}	R^2	mg·g^{-1}·(L·mg^{-1})$^{1/n}$	n	R^2
25	0.821 ± 0.053	32.669 ± 4.322	0.988	11.265 ± 1.090	2.884 ± 0.282	0.972
35	0.612 ± 0.066	30.230 ± 5.940	0.967	9.426 ± 1.072	2.705 ± 0.190	0.985
45	0.224 ± 0.016	32.819 ± 4.965	0.985	6.789 ± 1.099	2.342 ± 0.181	0.982
55	0.110 ± 0.007	35.311 ± 5.511	0.987	4.923 ± 1.131	2.049 ± 0.171	0.980

adsorbent dose of 8 g·L^{-1}. It can be seen that the maximum removal of MO was obtained at 25 °C. The removal decreased from 99.44 to 96.35, 99.12 to 94.33, 96.42 to 91.69, 92.79 to 84.92, and 84.02 to 78.22 % for the initial MO concentrations of (50, 100, 200, 300, and 400) mg·L^{-1}, respectively, by increasing the temperature from (25 to 55) °C. The decrease in dye adsorption with increasing temperature might be due to decreased surface activity with an increase in temperature. The result suggested that the adsorption between MO and CA was an exothermic process.

3.7. Adsorption Thermodynamics. In adsorption processes, thermodynamic parameters values are the actual indicators for practical application. Thermodynamic parameters such as free energy (ΔG^o), enthalpy (ΔH^o), and entropy (ΔS^o) change of adsorption can be determined from the following equations

$$\Delta G^o = \Delta H^o - T\Delta S^o \quad (2)$$

$$\Delta G^o = -RT \ln K_c \quad (3)$$

$$K_c = \frac{C_{Ae}}{C_e} \quad (4)$$

$$\ln K_c = \frac{\Delta S^o}{R} - \frac{\Delta H^o}{RT} \quad (5)$$

where ΔG^o, ΔH^o, and ΔS^o are changes in Gibbs free energy (kJ·mol^{-1}), enthalpy (kJ·mol^{-1}), and entropy (J·mol^{-1}·K^{-1}), respectively. K_c, C_{Ae}, C_e, R, and T are the equilibrium constant, the amount of MO adsorbed on the adsorbent of the solution at equilibrium (mg·L^{-1}), the equilibrium concentration of dye in the solution (mg·L^{-1}), the gas constant (8.314 J·mol^{-1}·K^{-1}), and the absolute temperature (K), respectively. The values of ΔH^o and ΔS^o are determined from the slope and the intercept of the plots of ln K_c versus $1/T$. The obtained thermodynamic parameter values are shown in Table 1. The negative values of ΔG^o indicate that the dye adsorption process is a spontaneous and exothermic process. The negative ΔH^o values suggest the exothermic nature of adsorption and the ΔS^o can be used to describe the randomness at the CA−solution interface during the adsorption.

3.8. Adsorption Isotherms. Adsorption isotherms are very important for the optimization of the adsorption system. The equilibrium relationship between absorbent and absorbate are best explained, and the maximum capacity of adsorption can be determined by the adsorption isotherm. There are several isotherm models available for analyzing experimental data and for describing the equilibrium of adsorption. Langmuir and Freundlich isotherm equations have been tested in this work.

The Langmuir isotherm model is based on the assumption of a structurally homogeneous adsorbent and a monolayer coverage with no interaction between the absorbate molecules. It is assumed that once the adsorbent site is covered with the dye molecules no further adsorption occurs at that site. It also suggests that all of the adsorption sites are of equivalent energy. The equation developed by Langmuir is expressed as follows:[22]

$$\frac{1}{q_e} = \frac{1}{q_m} + \frac{1}{K_L q_m C_e} \quad (6)$$

where q_e is the amount of dye adsorbed at the equilibrium (mg·g^{-1}), C_e is the supernatant concentration at the equilibrium state of the system (mg·L^{-1}), K_L is the Langmuir constant (L·mg^{-1}), and q_m is the maximum adsorption capacity (mg·g^{-1}).

The Freundlich isotherm model is based on the assumption that the adsorption occurs on heterogeneous surfaces with interaction between adsorbed molecules and suggests that adsorption energy has a nonuniform distribution over the adsorbent surface.[22] This isotherm is an empirical equation which can be employed to describe heterogeneous systems and is expressed as follows:

$$\log q_e = \log K_F + \frac{1}{n}\log C_e \quad (7)$$

where K_F is the Freundlich constant (L·g^{-1}) related to the bonding energy. K_F can be defined as the adsorption or distribution coefficient and represents the quantity of dye adsorbed onto adsorbent at unit equilibrium concentration, and n is the adsorption intensity or heterogeneity factor.

The equilibrium isotherm for the adsorption of dyes on adsorbent was determined. The parameters q_m, K_L, K_F, n, and R^2 are given in Table 2, and the graphical presentations for Langmuir and Freundlich adsorption isotherm are given in

dx.doi.org/10.1021/je2009945 | J. Chem. Eng.Data 2012, 57, 412−419

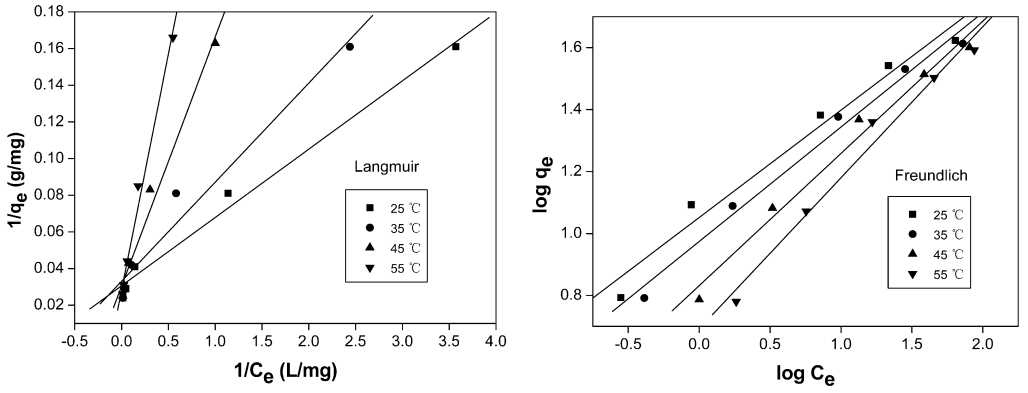

Figure 6. Langmuir and Freundlich adsorption isotherms for the MO-CA system.

Table 3. Adsorption Kinetic Constants and Correlation Coefficients Associated with Pseudofirst-Order and the Pseudosecond-Order Rate Equations at 25 °C

	pseudofirst-order rate equation			pseudosecond-order rate equation			
initial MO concentration	k_1	q_e,cal		k_2	q_e,cal	q_e,exp	
mg·L^{-1}	min^{-1}	mg·g^{-1}	R^2	g·mg^{-1}·min^{-1}	mg·g^{-1}	mg·g^{-1}	R^2
50	0.081 ± 0.027	0.558 ± 3.366	0.638	0.122 ± 0.035	6.342 ± 0.046	6.216	1.000
100	0.073 ± 0.004	2.943 ± 1.225	0.982	0.046 ± 0.007	12.695 ± 0.065	12.393	1.000
200	0.095 ± 0.018	24.843 ± 2.457	0.827	0.010 ± 0.002	25.374 ± 0.337	24.110	0.999
300	0.040 ± 0.010	6.199 ± 1.646	0.729	0.010 ± 0.002	35.817 ± 0.448	34.796	0.999
400	0.049 ± 0.009	10.142 ± 1.549	0.843	0.007 ± 0.001	43.592 ± 0.602	41.755	0.999

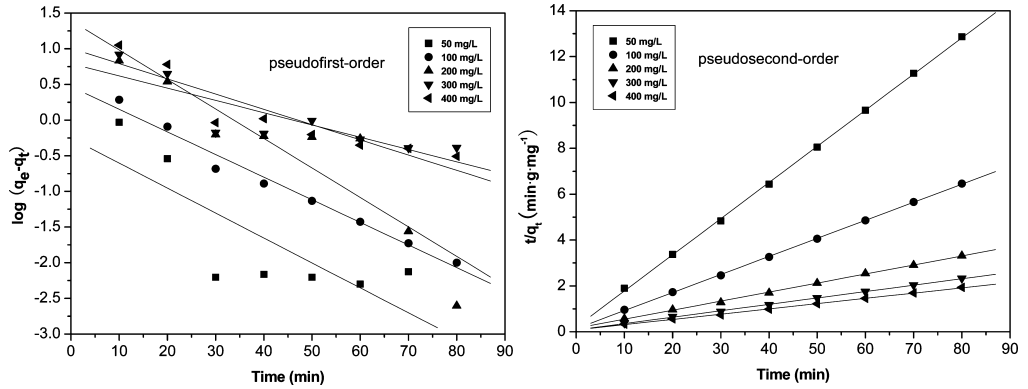

Figure 7. Pseudofirst-order and pseudosecond-order for the adsorption of MO onto CA at 25 °C.

Figure 6. It can be seen that the maximum monolayer adsorption capacities of the adsorbent are large in this study. This shows that the maximum adsorption capacity is highly dependent to the chemical structures of the dye and absorbents.

3.9. Adsorption Kinetics. To investigate the mechanism of adsorption, characteristic constants of adsorption were determined by using a pseudofirst-order equation of the Lagergren and Ho pseudosecond-order equation.[39,40] A linear form of pseudofirst-order model is:

$$\log(q_e - q_t) = \log(q_e) - \frac{k_1}{2.303}t \quad (8)$$

where q_e is the amount of dye adsorbed at equilibrium (mg·g^{-1}), q_t is amount of dye adsorbed at a time t (mg·g^{-1}), and k_1 is the rate constant of pseudofirst-order kinetics (min^{-1}). The rate constant, k_1, and correlation coefficients (R^2) of the dye under different concentrations were calculated from the linear plots of $\log(q_e - q_t)$ versus t.

The kinetic data were also analyzed using Ho's pseudo-second-order kinetics model. A linear form of pseudosecond-order model is as follows:

$$\frac{t}{q_t} = \frac{1}{k_2 q_e^{\,2}} + \frac{1}{q_e}t \quad (9)$$

where k_2 is the rate constant of pseudosecond-order (g·mg^{-1}·min^{-1}). There would be a good linear relationship between the t/q_t and contact time (t) if pseudosecond-order kinetics is applicable for the adsorption process. k_2 and q_e can be determined from the slope and intercept of the plot t/q_t versus t, respectively. All of the parameters mentioned above are determined and listed in Table 3. The graphical presentations for pseudofirst- and pseudosecond-order kinetics model are given in Figure 7. It can be seen that the correlation coefficients for the pseudofirst-order kinetic model are low. Moreover, a large difference of equilibrium adsorption capacity

dx.doi.org/10.1021/je2009945 | J. Chem. Eng.Data 2012, 57, 412–419

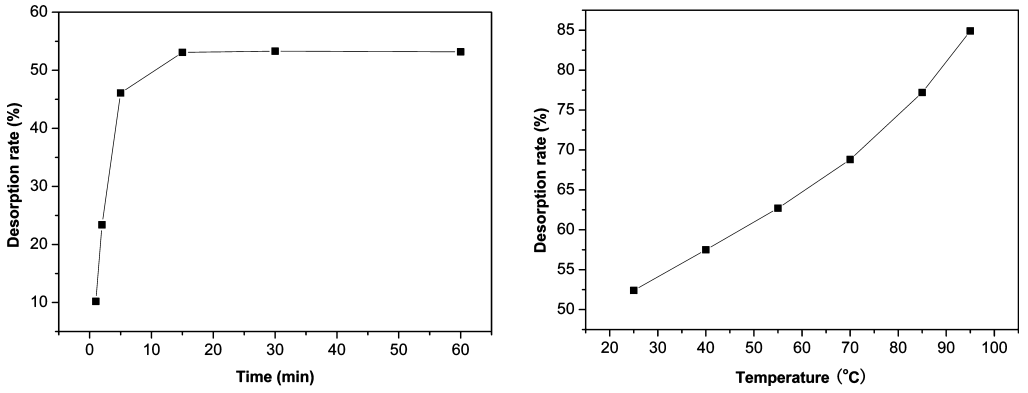

Figure 8. Effects of time and temperature on the desorption rate (%).

(q_e) between the experiment and the calculation was observed, indicating a poor pseudofirst-order fit to the experimental data.

The results of pseudosecond-order kinetics showed that the linear fit with extremely high correlation coefficients (R^2 > 0.999) were obtained for all studied initial dye concentrations. Moreover, the calculated q_e values also fairly agree with the experimental data in the case of pseudosecond-order kinetics. These results show that the rates of adsorption conform to pseudosecond-order kinetics. The calculated q_e values increased with an increase in the initial dye concentration, and the rate constants varied over a wide range, suggesting that limiting steps may be chemisorption through the sharing and exchange of electrons between the sorbent and the substrate. That the values of the rate constant k decrease with increasing initial dye concentration can be attributed to the lower competition for the sorption surface sites at lower concentrations. At higher concentrations, the competition for the surface active sites will be high, and consequently lower sorption rates are obtained.

3.10. Desorption Studies. The effects of time and temperature on the desorption of MO from CA are shown in Figure 8. It was apparent that MO desorption increased with increasing time and temperature. The speed of desorption of MO was rapid, and the solution could reach equilibrium rapidly. The maximum desorption rate of MO was 84.91% at high temperature.

4. CONCLUSIONS

The results obtained from this study show that CA can be an alternate adsorbent for MO removal from aqueous solution. The effect of pH of aqueous solution decreases the removal efficiency with the increase in pH due to the ionic effects. The % MO removal increases from (56.33 to 99.34) % for an increase in adsorbent dose from (1 to 12) g·L^{-1} because of the concentration gradient between MO concentration in the solution and the MO concentration in the surface of the CA. The increase in initial dye concentration also enhances the interaction between MO and CA which results in a decreased percentage of MO removal with the increase in initial concentration of MO. In the effect of contact time, the percentage removal increases with time up to 90 min and remains almost constant. The temperature has an adverse effect on the percentage of dye removal due to the decreased surface activity suggesting that adsorption between MO and CA was an exothermic process. The equilibrium data have been analyzed using Langmuir and Freundlich isotherms. The characteristic parameters for each isotherm and related correlation coefficients have been determined. The thermodynamic analysis indicates that the system is spontaneous and exothermic. The suitability of the pseudofirst- and pseudo-second-order kinetic models for the sorption of MO onto CA is also discussed. The pseudosecond-order kinetic model agrees very well with the dynamic behavior for the adsorption of MO onto CA for different initial MO concentrations over the whole range studied. The study will be useful for using the novel materials as a low-cost adsorbent for the removal of azo dyes.

AUTHOR INFORMATION

Corresponding Author

*Tel.: +86-316-2188377. E-mail: zhangjixiang1973@163.com.

Funding

The authors are grateful for the financial support by the Youth Science Foundation of Hebei Province (No. 2010156) and the Nature Science Foundation of Langfang Teachers' College (No. LSZB201001).

REFERENCES

(1) Mahmoodi, N. M.; Hayati, B.; Arami, M.; Lan, C. Adsorption of textile dyes on pine cone from colored wastewater: Kinetic, equilibrium and thermodynamic studies. *Desalination* **2011**, *268*, 117−125.

(2) Türgay, O.; Ersöz, G.; Atalay, S.; Fross, J.; Welander, U. The treatment of azo dyes found in textile industry wastewater by anaerobic biological method and chemical oxidation. *Sep. Purif. Technol.* **2011**, *79*, 26−33.

(3) Gudelj, I.; Hrenović, J.; Dragičević, T. L.; Delaš, F.; Soljan, V.; Gudelj, H. Azo dyes, their environmental effects, and defining a strategy for their biodegradation and detoxification. *Arh. Hig. Rada Toksikol.* **2011**, *62*, 91−101.

(4) He, H. Y.; Huang, J. F.; Cao, L. Y.; Wu, J. P. Photodegradation of methyl orange aqueous on $MnWO_4$ powder under different light resources and initial pH. *Desalination* **2010**, *252*, 66−70.

(5) Parshetti, G. K.; Telke, A. A.; Kalyani, D. C.; Govindwar, S. P. Decolorization and detoxification of sulfonated azo dye methyl orange by Kocuria rosea MTCC 1532. *J. Hazard. Mater.* **2010**, *176*, 503−509.

(6) Gomathi, D. L.; Mohan, R. K. Enhanced photocatalytic activity of silver metallized TiO_2 particles in the degradation of an azo dye methyl orange: Characterization and activity at different pH values. *Appl. Surf. Sci.* **2010**, *256*, 3116−3121.

(7) Teng, M. Y.; Lin, S. H. Removal of methyl orange dye from water onto raw and acid-activated montmorillonite in fixed beds. *Desalination* **2006**, *201*, 71−81.

(8) Ghoneim, M. M.; El-Desoky, H. S.; Zidan, N. M. Electro-Fenton oxidation of Sunset Yellow FCF azo-dye in aqueous solutions. *Desalination* **2011**, *274*, 22−30.

(9) Zanjanchi, F. Photo-oxidation of phenylazonaphthol dyes and their reactivity analysis in the gas phase and adsorbed on cellulose fibers states using DFT and TD-D. *Dyes Pigm.* **2011**, *89*, 16−22.
(10) Yavuz, Y.; Koparal, A. S.; Öğütveren, Ü. B. Electrochemical oxidation of Basic Blue 3 dye using a diamond anode: evaluation of colour, COD and toxicity removal. *J. Chem. Technol. Biotechnol.* **2011**, *86*, 261−265.
(11) Zahrim, A. Y.; Tizaoui, C.; Hilal, N. Removal of Highly Concentrated Industrial Grade Leather Dye: Study on Several Flocculation and Sand Filtration Parameters. *Sep. Sci. Technol.* **2011**, *46*, 883−892.
(12) Andersen, N. P. R; Christensen, M. L.; Keiding, K. Investigation of filtration conditions for nanofiltration of reactive dye printing wastewater. *Filtration* **2007**, *7*, 75−81.
(13) Koyuncu, I. Direct filtration of Procion dye bath wastewaters by nanofiltration membranes: flux and removal characteristics. *J. Chem. Technol. Biotechnol.* **2004**, *78*, 1219−1224.
(14) Nourouzi, M. M.; Chuah, T. G.; Choong, T. S. Optimisation of reactive dye removal by sequential electrocoagulation-flocculation method: comparing ANN and RSM prediction. *Water Sci. Technol.* **2011**, *63*, 984−994.
(15) Sadri Moghaddam, S.; Alavi Moghaddam, M. R.; Arami, M. Coagulation/flocculation process for dye removal using sludge from water treatment plant: Optimization through response surface methodology. *J. Hazard. Mater.* **2010**, *175*, 651−657.
(16) Riera-Torres, M.; Gutiérrez-Bouzán, C.; Crespi, M. Combination of coagulation−flocculation and nanofiltration techniques for dye removal and water reuse in textile effluents. *Desalination* **2010**, *252*, 53−59.
(17) Nandi, S. P.; Walker, P. L. Jr. Adsorption of dyes from aqueous solution by coals, chars, and active carbons. *Fuel* **1971**, *50*, 345−366.
(18) Hamdi, M. H. G.; Abd. El-Hakim, A. M. D. Impact of Surface Chemistry on the Removal of Indigo Carmine Dye Using Apricot Stone Active Carbon. *Adsorpt. Sci. Technol.* **2007**, *25*, 327−341.
(19) Chan, L. S.; Cheung, W. H.; Allen, S. J.; McKay, G. Separation of acid-dyes mixture by bamboo derived active carbon. *Sep. Purif. Technol.* **2009**, *67*, 166−172.
(20) Rashed, M. N. Acid dye removal from industrial wastewater by adsorption on treated sewage sludge. *Int. J. Environ. Waste Manage.* **2011**, *7*, 175−191.
(21) Madhavakrishman, S.; Manickavasagam, K.; Vasanthakumar, R.; Rasappan, K.; Mohanraj, R.; Pattabhi, S. Adsorption of crystal violet dye from aqueous solution using *ricinus communis* pericarp carbon as an adsorbent. *E-J Chem.* **2009**, *6*, 1109−1116.
(22) Mittal, A.; Mittal, J.; Malviya, A.; Kaur, D.; Gupta, V. K. Adsorption of hazardous dye crystal violet from wastewater by waste materials. *J. Colloid Interface Sci.* **2010**, *343*, 463−473.
(23) Saeeda, A.; Sharif, M.; Iqbal, M. Application potential of grapefruit peel as dye sorbent: Kinetics, equilibrium and mechanism of crystal violet adsorption. *J. Hazard. Mater.* **2010**, *179*, 564−572.
(24) Khattri, S. D.; Singhb, M. K. Removal of malachite green from dye wastewater using neem sawdust by adsorption. *J. Hazard. Mater.* **2009**, *167*, 1089−1094.
(25) Gupta, V. K.; Jain, R.; Shrivastava, M.; Navak, A. Equilibrium and thermodynamic studies on the adsorption of the dye tartrazine onto waste "coconut husks" carbon and activated Carbon. *J. Chem. Eng. Data* **2010**, *55*, 5083−5090.
(26) Belala, Z.; Jeguirim, M.; Belhachemi, M.; Addoun, F.; Trouvé, G. Biosorption of basic dye from aqueous solutions by Date Stones and Palm-Trees Waste: Kinetic, equilibrium and thermodynamic studies. *Desalination* **2011**, *271*, 80−87.
(27) Nandi, B. K.; Goswami, A.; Das, A. K.; Mondal, B.; Purkait, M. K. Kinetic and equilibrium studies on the adsorption of crystal violet dye using Kaolin as an adsorbent. *Sep. Sci. Technol.* **2008**, *43*, 1382−1403.
(28) Gupta, V. K.; Jain, R.; Siddiqui, M. N.; Saleh, T. A.; Agarwal, S.; Malati, S.; Pathak, D. Equilibrium and Thermodynamic Studies on the Adsorption of the Dye Rhodamine-B onto Mustard Cake and Activated Carbon. *J. Chem. Eng. Data* **2010**, *55*, 5225−5229.
(29) Rodríguez, A.; Ovejero, G.; Mestanza, M.; García, J. Removal of Dyes from Wastewaters by Adsorption on Sepiolite and Pansil. *Ind. Eng. Chem. Res.* **2010**, *49*, 3207−3216.
(30) Wang, S.; Yu, D.; Huang, Y.; Guo, J. The adsorption of sulphonated azo-dyes methyl orange and xylenol orange by coagulation on hollow chitosan microsphere. *J. Appl. Polym. Sci.* **2011**, *119*, 2065−2071.
(31) Wang, L.; Zhang, J.; Wang, A. Fast removal of methylene blue from aqueous solution by adsorption onto chitosan-g-poly (acrylic acid)/attapulgite composite. *Desalination* **2011**, *266*, 33−39.
(32) Dotto, G. L.; Pinto, L. A. A. Adsorption of food dyes onto chitosan: Optimization process and kinetic. *Carbohyd. Polym.* **2011**, *84*, 231−238.
(33) Kittinaovarat, S.; Kansomwan, P.; Jiratumnukul, N. Chitosan/modified montmorillonite beads and adsorption Reactive Red 120. *Appl. Clay Sci.* **2010**, *48*, 87−91.
(34) Huang, X. Y.; Mao, X. Y.; Bu, H. T.; Yu, X. Y.; Jiang, G. B.; Zeng, M. H. Chemical modification of chitosan by tetraethylenepentamine and adsorption study for anionic dye removal. *Carbohyd. Res.* **2011**, *346*, 1232−1240.
(35) Boddu, V. M.; Abburi, K. A.; Talbott, J. L.; Smith., E. D. Removal of hexavalent chromium from wastewater using new composite chitosan biosorbent. *Environ. Sci. Technol.* **2003**, *37*, 4449−4456.
(36) Futalan, C. M.; Kan, C. C.; Dalida, M. L.; Hsien, K. J.; Pascua, C.; Wan, M. W. Comparative and competitive adsorption of copper, lead, and nickel using chitosan immobilized on bentonite. *Carbohyd. Polym.* **2011**, *83*, 528−536.
(37) Kamari, A.; Ngah, W. S. W. Isotherm, kinetic and thermodynamic studies of lead and copper uptake by H_2SO_4 modified chitosan. *Colloid Surf., B* **2009**, *73*, 257−266.
(38) Yang, Y. M.; Wang, J. W.; Tan, R. X. Immobilization of glucose oxidase on chitosan−SiO_2 gel. *Enzyme Microb. Technol.* **2004**, *34*, 126−131.
(39) Nandi, B. K.; Goswami, A.; Purkait, M. K. Removal of cationic dyes from aqueous solutions by kaolin: kinetic and equilibrium studies. *Appl. Clay Sci.* **2009**, *42*, 583−590.
(40) Barka, N.; Assabbane, A.; Nounah, A.; Laanab, L.; AîtIchou, Y. Removal of textile dyes from aqueous solutions by natural phosphate as a new adsorbent. *Desalination* **2009**, *235*, 264−275.